Visualization of CD2 Interaction with LFA-3 and Determination of the Two-Dimensional Dissociation Constant for Adhesion Receptors in a Contact Area

Michael L. Dustin,* Laura M. Ferguson,‡ Po-Ying Chan,§¶ Timothy A. Springer,§¶ and David E. Golan‡‖**

*Center for Immunology and Department of Pathology, Washington University School of Medicine, St. Louis, Missouri 63110; and Departments of ‡Biological Chemistry and Molecular Pharmacology, §Pathology, and ‖Medicine, Harvard Medical School; ¶Center for Blood Research; and **Hematology-Oncology Division, Brigham and Women's Hospital, Boston, Massachusetts 02115

Abstract. Many adhesion receptors have high three-dimensional dissociation constants (K_d) for counter-receptors compared to the K_ds of receptors for soluble extracellular ligands such as cytokines and hormones. Interaction of the T lymphocyte adhesion receptor CD2 with its counter-receptor, LFA-3, has a high solution-phase K_d (16 μM at 37°C), yet the CD2/LFA-3 interaction serves as an effective adhesion mechanism. We have studied the interaction of CD2 with LFA-3 in the contact area between Jurkat T lymphoblasts and planar phospholipid bilayers containing purified, fluorescently labeled LFA-3. Redistribution and lateral mobility of LFA-3 were measured in contact areas as functions of the initial LFA-3 surface density and of time after contact of the cells with the bilayers. LFA-3 accumulated at sites of contact with a half-time of ~15 min, consistent with the previously determined kinetics of adhesion strengthening. The two-dimensional K_d for the CD2/LFA-3 interaction was 21 molecules/μm^2, which is lower than the surface densities of CD2 on T cells and LFA-3 on most target or stimulator cells. Thus, formation of CD2/LFA-3 complexes should be highly favored in physiological interactions. Comparison of the two-dimensional (membrane-bound) and three-dimensional (solution-phase) K_ds suggest that cell–cell contact favors CD2/LFA-3 interaction to a greater extent than that predicted by the three-dimensional K_d and the intermembrane distance at the site of contact. LFA-3 molecules in the contact site were capable of lateral diffusion in the plane of the phospholipid bilayer and did not appear to be irreversibly trapped in the contact area, consistent with a rapid off-rate. These data provide insights into the function of low affinity interactions in adhesion.

MULTICELLULAR organisms use cell contact and adhesion for both structural integrity and short range communication. In the immune system, adhesion of T cells to antigen presenting cells (APCs)[1] is mediated by antigen receptors and adhesion receptors. The T cell antigen receptor and the accessory molecules CD4 and CD8 (cluster of differention antigens 4 and 8) bind directly to antigenic peptide: major histocompatibility complex (MHC) protein adducts (15, 24, 31). Parallel interactions involving CD2 with lymphocyte function-associated antigen 3 (LFA-3) and LFA-1 with ICAMs 1, 2, and 3 are required for stable cell–cell adhesion (14, 18, 40). CD2 and LFA-3 are members of the immunoglobulin superfamily (IgSF), each possessing two Ig-like domains, that bind to each other through an interaction involving their NH_2-terminal Ig-like domains (1, 20, 32, 39). If the mode of interaction between CD2 and LFA-3 is similar to that employed by other adhesion molecules of the IgSF, then the CD2/LFA-3 interaction may serve as a prototype for adhesive interactions involved in neural cell adhesion, cell migration in development and tumor cell metastasis.

The CD2/LFA-3 interaction was the first heterophilic adhesion mechanism to be fully reconstituted (17, 37, 41). It was also the first heterophilic mechanism for which the solution-phase interaction was rigorously analyzed. The dissociation constant (K_d) and off-rate for the interaction

Address correspondence to David E. Golan, M.D., Ph.D., Department of Biological Chemistry and Molecular Pharmacology, Harvard Medical School, 250 Longwood Avenue, Boston, MA 02115. Tel.: (617) 432-2256. FAX: (617) 432-3833 or Michael L. Dustin, Ph.D., Department of Pathology, Washington University School of Medicine, 660 South Euclid Avenue, Box 8118, St Louis, MO 63110. Tel.: (314) 362-9618. FAX: (314) 362-8888.

1. *Abbreviations used in this paper*: APC, antigen presenting cell; CD2, cluster of differentiation antigen 2; FPR, fluorescence photobleaching recovery; GPI–LFA-3, glycosyl-phosphatidylinositol-linked LFA-3; IgSF, immunoglobulin superfamily; LFA-3, lymphocyte function-associated antigen 3; MHC, major histocompatibility complex; OG, octyl-β-D-glucopyranoside; PC, phosphatidylcholine; TCR, T cell antigen receptor; TM–LFA-3, transmembrane LFA-3.

between purified soluble forms of CD2 and LFA-3 are 1.6 $\times 10^{-5}$ M and greater than 4 s^{-1}, respectively (45). It has been suggested that the high K_d and fast off-rate of the CD2/LFA-3 interaction allows for cell–cell dissociation, which is essential for the migration of long-lived T lymphocytes (44).

Before the description of heterophilic adhesion mechanisms such as that involving CD2 and LFA-3, the three part interaction among cellular Fc receptors, hapten-specific antibody, and hapten-coated surfaces or liposomes provided an important model for molecular studies of adhesion. A classic study by McCloskey and Poo (26) showed that the interaction of a cell bearing fluorescently labeled anti-DNP antibody-IgεFc receptor complexes with a liposome incorporating DNP-labeled phospholipids efficiently drove accumulation of antibody-Fc receptor complexes into the area of contact between the cell and the liposome. This "trapping" effect correlated with adhesion strengthening. Receptor accumulation did not require an active contribution from the cell, suggesting that it was driven by the extracellular binding interaction ($K_d = 10^{-8}$ M) between antibody and DNP. Although this study did demonstrate the importance of adhesion molecule trapping in contact areas as a general mechanism, it did not determine an upper limit for the K_d of an interaction that could be mediated by this trapping or syn-capping effect. This is an important question, since the CD2/LFA-3 interaction functions in adhesion with a solution-phase K_d of 16 μM. Other studies showing redistribution of adhesion molecules to contact areas have not excluded (or have specifically invoked) interactions with the cytoskeleton as a contributing or necessary process in adhesion receptor accumulation (10, 11, 21, 22, 28, 30, 48). Therefore, such studies do not directly address the role of the K_d of adhesion receptor interactions in receptor redistribution.

We have previously shown that a glycosylphosphatidylinositol anchored isoform of LFA-3 (GPI–LFA-3) is more potent than a transmembrane isoform in mediating adhesion of $CD2^+$ T lymphoblasts to glass-supported planar bilayers reconstituted with LFA-3 (9). This difference in potency is related to the observation that transmembrane proteins are laterally immobile (9, 27), whereas phospholipids (9, 27) and GPI-anchored proteins (9) are laterally mobile, in glass-supported planar bilayers. One likely mechanism for the effect of lateral diffusion on adhesion involves an increase in the rate of productive collisions between laterally mobile LFA-3 and CD2. A second likely mechanism involves trapping of laterally mobile LFA-3 in the contact area, which increases the effective LFA-3 density. In the present study we have labeled purified GPI–LFA-3 with FITC, incorporated FITC-LFA-3 into glass-supported planar bilayers, and characterized changes in the surface distribution and diffusion coefficient of LFA-3 induced by interaction with $CD2^+$ T lymphoblasts. We find that LFA-3 accumulates in contact areas with T lymphoblasts. Equilibrium binding analysis shows that the two-dimensional K_d for the CD2/LFA-3 interaction is low relative to the normal surface densities of CD2 and LFA-3 in biological membranes, suggesting that binding approaches saturation in biological contact areas. Comparison between two- and three-dimensional K_ds for the CD2/LFA-3 interaction suggests that CD2 and LFA-3 are under topological constraints such as those described by Bell et al. (4) as a "confinement region", or a thin subregion of volume within the contact area in which adhesion molecule binding sites are localized. Finally, we detect lateral diffusion of "bound" LFA-3 in the contact area, consistent with a rapid off-rate for the CD2/LFA-3 binding interaction.

Materials and Methods

Monoclonal Antibodies and Cell Lines

The monoclonal antibodies TS2/9 (anti-LFA-3) and TS2/18 (anti-CD2) were originally described in Sanchez-Madrid et al. (34). The Jurkat T lymphoma cell line was maintained in RPMI 1640 containing 10% fetal bovine serum, 5 mM glutamine and 50 μg/ml gentamicin. Jurkat cells in log phase of growth (6–9 $\times 10^5$ cells/ml) were used for all experiments.

Purification and Modification of LFA-3

GPI–LFA-3 was affinity-purified from human erythrocytes, as previously described (17). To avoid modification of the CD2 binding surface on critical lysines, LFA-3 was bound to TS2/9-coupled Sepharose CL-4B before conjugation with FITC. Purified LFA-3 was added in a sufficient amount to saturate 1 ml of TS2/9 Sepharose CL-4B (2 mg/ml) in neutralized elution buffer, and the mixture was rotated at 4°C for 4–16 h. The Sepharose was washed extensively at 4°C in 0.1 M $NaHCO_3/Na_2CO_3$, pH 9.0, 0.05% Triton X-100, and excess buffer was removed. FITC was dissolved in dimethylformamide to a concentration of 80 mM, and the solution was diluted 1:9 in 1 ml of 0.1 M $NaHCO_3/Na_2CO_3$, pH 9.0, 0.05% Triton X-100 and added immediately to the LFA-3 TS2/9 Sepharose mixture. After 2 h of end over end rotation at room temperature the slurry was centrifuged, the supernatant was removed, a fresh preparation of 8 mM FITC in 0.1 M $NaHCO_3/Na_2CO_3$, pH 9.0, 0.05% Triton X-100 was added, and the room temperature incubation was repeated. The slurry was transferred to a column and washed with 50 volumes of 25 mM Tris, pH 8.6, 0.15 M NaCl, 1% octyl-β-D-glucopyranoside (OG). FITC-modified LFA-3 (FITC–LFA-3) was eluted with 50 mM glycine, pH 3.0, 0.15 M NaCl, 1% OG and collected in tubes containing 1 M Tris, pH 8.6, 1% OG.

Preparation of Liposomes and Planar Bilayers

Unilamellar liposomes were prepared by OG dialysis (7,29). Egg phosphatidylcholine (PC) (Avanti Polar Lipids, Inc., Pelham, AL) was dissolved at 0.4 mM in 25 mM Tris, pH 8.0, 0.15 M NaCl, 2% OG, and then mixed with an equal volume of 25 mM Tris, pH 8.0, 0.15 M NaCl, 2% OG containing different amounts of LFA-3 or FITC–LFA-3. Liposome suspensions were formed by dialysis and stored at 4°C under argon to minimize lipid oxidation.

Planar bilayers containing purified LFA-3 or FITC–LFA-3 were formed as previously described (17), with the following modifications. In some experiments, bilayers were formed from a mixture of liposomes containing FITC–LFA-3 and purified LFA-1 (16). A diamond pencil was used to place a shallow scratch in the center of clean coverslips to permit identification of the plane of the bilayer. In a 2-l tank of 25 mM Hepes, pH 7.4, 147 mM NaCl, 5 mM glucose, 1% bovine serum albumin (HBS), the planar bilayer bearing coverslips were transferred to glass slides that had been coated with 10-mm rings of vacuum grease (Dow-Corning, Corning, NY). A Jurkat cell suspension was pipetted within the grease ring just as the coverslip was slowly lowered and pressed into the grease to trap a small number of cells. The incubation was initiated when the system was inverted coverslip down. In some cases, CD2 molecules on Jurkat cells were blocked by preincubating cells with TS2/18 at 100 μg/ml for 30 min and washing three times with HBS. Cells were incubated with bilayers at room temperature. LFA-3 site densities on planar bilayers were determined by radioimmunoassay, as previously described (9).

Fluorescence Photobleaching Recovery

Fluorescence photobleaching recovery (FPR) is used to measure the lateral mobility of fluorescently labeled proteins and lipids in membranes (2). Spot FPR was performed on a Meridian Instruments (Okemos, Michigan) ACAS 570 Interactive Laser Cytometer. Data were analyzed using a nonlinear least squares method (5) to yield both the lateral diffusion coef-

ficient and the fraction of fluorescently labeled molecules that were free to diffuse on the time scale of the experiment (typically 45–90 s). The ACAS 570 uses a computer-interfaced scanning stage to generate line scans through the bleach site that are used to monitor non-bleached regions of the bilayer as an internal control. Bleaching pulses were 30–100 ms in duration using a beam power of 200 μW. Measuring pulses were 4 μs in duration using a beam power of 100–225 μW. The $1/e^2$ diameter of the laser beam was measured as 1.3 ± 0.07 μm (mean ± SD, $n = 6$) using a 40× 1.3 N.A. oil immersion objective. Non-FITC fluorescence was excluded from the emission detection system by using a 530 ± 15 nm band pass filter. The fluorescence signal from unlabeled bilayers was less than 10% of that from labeled bilayers, and was subtracted from the total signal.

Image Analysis

Two-dimensional fluorescence images of FITC–LFA-3 distribution in egg PC planar bilayers were obtained using the Meridian ACAS 570. Most images were taken as 90 × 90-μm fields using a step size of 0.5 μm. Bright field images of Jurkat cells on bilayers were used to draw outlines of the cells (i.e., cell profiles) on the fluorescence images. These outlines were used to determine projected cell areas and to define areas of the bilayer not in contact with cells. Projected cell area was defined as the area of a disk in the horizontal plane through the widest part of the cell. Contact sites were defined mathematically to include all pixels having fluorescence values ≥120% of the average pixel intensity outside the cell outlines. The average autofluorescence of Jurkat cells adherent to unlabeled LFA-3 in egg PC planar bilayers was subtracted as a background. Average fluorescence intensities within areas of cell contact and non-cell contact were converted to LFA-3 surface densities by setting the average fluorescence intensity in multiple fields of FITC–LFA-3 equal to the surface density of LFA-3 measured by iodinated antibody binding. When laser power and photomultiplier tube gain were held constant, there was a linear relationship between fluorescence intensity (arbitrary units) and LFA-3 site density determined by radioimmunoassay over the range used in these experiments (data not shown).

Bound receptor densities were determined using conventions for equilibrium dialysis (43). All data were corrected for background by subtraction of fluorescence signals from planar bilayers without FITC–LFA-3 or from cells adherent to bilayers containing unlabeled LFA-3, as appropriate. The density of free LFA-3 in the bilayer (i.e., of LFA-3 not interacting with cells) was determined from the average LFA-3 density outside the cell outlines. The density of bound LFA-3 in a contact site was defined as the average LFA-3 density within the contact site minus the free LFA-3 density in the bilayer. The total number of bound LFA-3 molecules was determined by integrating the density of bound LFA-3 over the contact area.

Two-Dimensional Scatchard Analysis

LFA-3 surface densities, determined as described above, were plotted as bound on the abscissa and bound/free on the ordinate. Linear least squares analysis was used to determine the slope, which is proportional to the negative reciprocal of the two-dimensional K_d (mol/μm^2). Extrapolation to the abscissa was used to determine the binding at saturation (mol/μm^2 of contact area) (35).

Results

Redistribution of LFA-3 into Areas of Planar Bilayers in Contact with Jurkat T Cells

GPI–LFA-3 was purified from human erythrocytes by immunoaffinity chromatography. FITC was conjugated to LFA-3 bound to a Sepharose-coupled antibody that blocks interaction with CD2, to protect the CD2-binding site from modification by fluorophore. FITC–LFA-3 was incorporated into phospholipid liposomes which were then

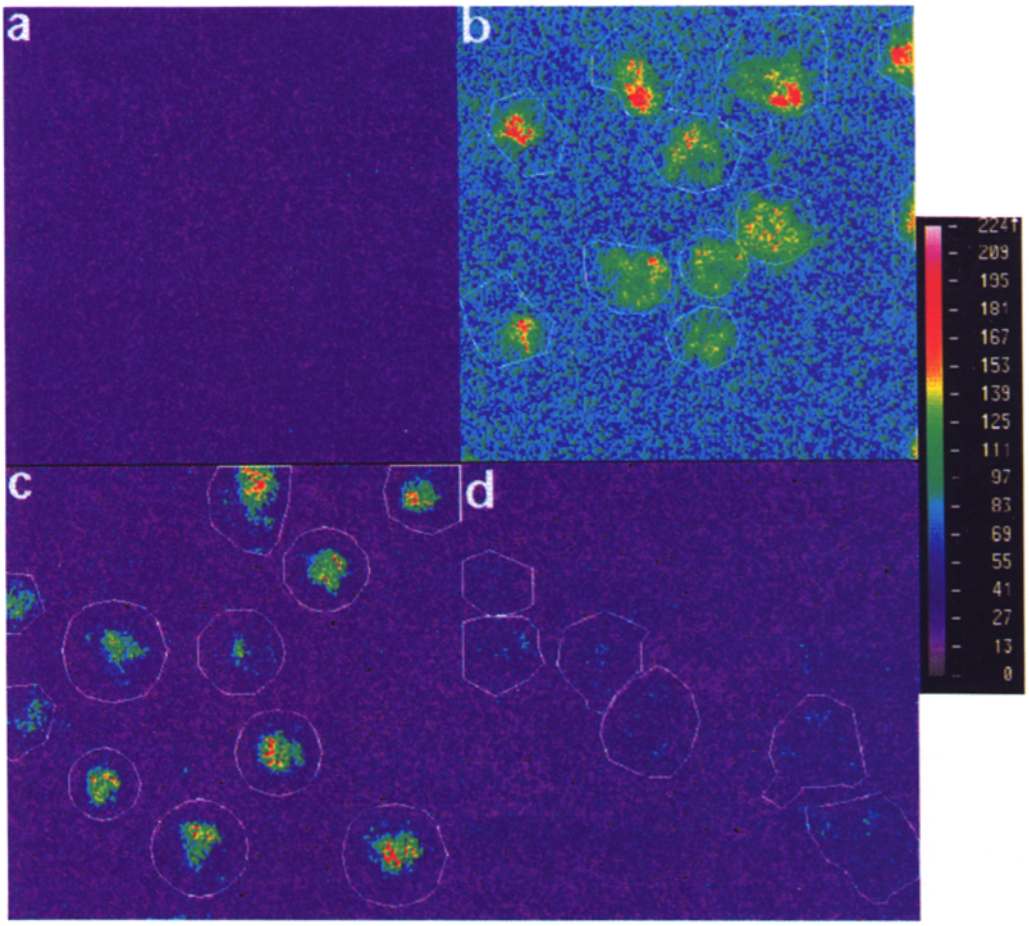

Figure 1. Pseudocolor fluorescence images of FITC-LFA-3 distribution in glass-supported planar bilayers. (*a*) Uniform distribution of FITC–LFA-3 (120 mol/μm^2) in a planar bilayer before interaction with cells. (*b*) Distribution of FITC–LFA-3 (initial density, 1,000 mol/μm^2) in a planar bilayer 30 min after incubation with Jurkat T cells. (*c*) Distribution of FITC–LFA-3 (initial density, 120 mol/μm^2) in a planar bilayer 30 min after incubation with Jurkat T cells. (*d*) Distribution of fluorescence in a planar bilayer containing 120 mol/μm^2 of FITC–LFA-3 and 500 mol/μm^2 of unlabeled LFA-1 30 min after incubation with TS2/18 pretreated Jurkat T cells. The projections of attached cells are outlined in white. The pseudocolor scale is marked in arbitrary fluorescence units. Each image represents 8,100 μm^2.

allowed to interact with glass coverslips to form planar phospholipid bilayers on the glass surface. Quantitative fluorescence imaging revealed a uniform distribution of FITC–LFA-3 in the planar bilayers (Fig. 1 *a*).

Upon incubation of planar bilayers with $CD2^+$ Jurkat T cells, FITC–LFA-3 redistributed into areas of contact with cells (Fig. 1, *b* and *c*, see also Figs. 4 and 5). The following experiment demonstrated that FITC–LFA-3 redistribution required specific interaction with CD2 on T cells. Jurkat cells were allowed to adhere to planar bilayers formed by mixtures of liposomes containing FITC–LFA-3 and purified LFA-1 in the presence of Mg^{2+}. LFA-1 dependent adhesion, mediated by binding of LFA-1 to ICAMs on the Jurkat cells, had no effect on FITC–LFA-3 redistribution into the contact areas. Blocking of CD2 molecules on the Jurkat cells with TS2/18, a mAb known to block interaction of CD2 with LFA-3, prevented redistribution of FITC–LFA-3 into the LFA-1–mediated contact areas (Fig. 1 *d*).

Kinetics of Contact Area Development

Contact areas were defined operationally as areas of significantly increased LFA-3 accumulation. Fig. 2 shows the size of contact areas and the average density of bound LFA-3 within contact areas as a function of time after incubation of Jurkat cells with planar bilayers initially presenting 120 LFA-3 mol/μm^2. The mean size of the contact areas increased rapidly over the first 28 min of incubation and then leveled off at an average size of 98 μm^2. Likewise, the density of bound LFA-3 in the contact areas increased steadily over the first 31 min before leveling off at an average density of 330 mol/μm^2. Similar kinetics of contact area expansion were observed with bilayers initially presenting 120 (Fig. 2), 300, and 1,000 LFA-3 mol/μm^2 (not shown).

Dependence of Bound LFA-3 Density on Cell Size

Jurkat cells display size heterogeneity in log phase cultures. The effect of this heterogeneity on FITC–LFA-3 accumulation was assessed. FITC–LFA-3 fluorescence images were analyzed with respect to projected cell area obtained from matched bright-field images. Although larger cells formed larger contact areas within the planar bilayer, the average density of LFA-3 within these contact areas was the same as that in the contact areas formed by smaller cells (Fig. 3).

The spatial distribution of LFA-3 within contact areas was also analyzed. Most cells generated contact areas with a single, central area of concentrated ligand and decreasing ligand density toward the periphery (see Figs. 4 and 5). Peak fluorescence value within a contact area was defined as the greatest fluorescence value held by at least four adjacent pixels (i.e., by an area of at least 1 μm^2). The maximum density of bound FITC–LFA-3 was 1,000 mol/μm^2.

Lateral Diffusion of LFA-3 in Contact Areas

Fluorescence photobleaching recovery was used to measure the fraction of FITC–LFA-3 that was free to diffuse in the planar bilayer (i.e., the fractional mobility) and the lateral diffusion coefficient of the mobile fraction (Figs. 4 and 5; Table I). Fig. 4 shows the time course of fluores-

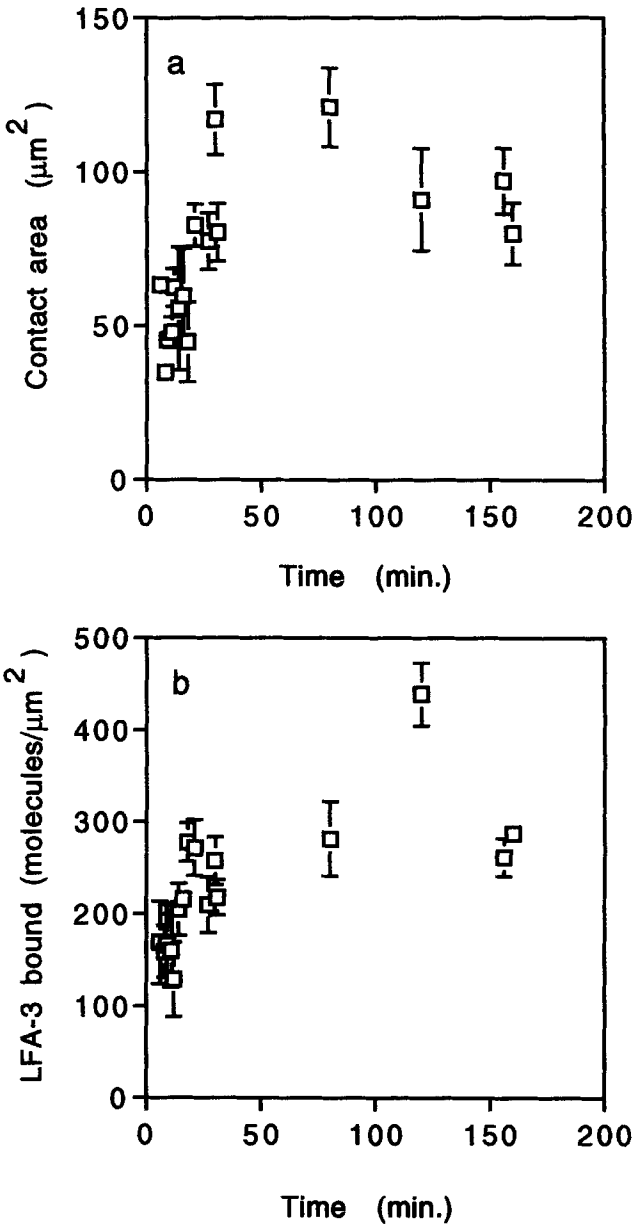

Figure 2. Kinetics of FITC–LFA-3 interaction with Jurkat T cells. Jurkat cells were allowed to adhere for various lengths of time to planar egg PC bilayers containing FITC–LFA-3. Fluorescence images were analyzed for (*a*) size of contact area (μm^2) and (*b*) density of bound FITC–LFA-3 in contact area (mol/μm^2). Data were taken on planar bilayers initially presenting 120 LFA-3 mol/μm^2. Each experimental point represents mean ± SEM for all contact areas in a single microscope field.

cence recovery following photobleaching of FITC–LFA-3 in a contact area between a Jurkat T cell and a planar bilayer initially presenting 120 LFA-3 mol/μm^2. Fig. 5 shows prebleach, 0 s post-bleach and 90 s post-bleach line scans of FITC–LFA-3 fluorescence in contact areas between cells and bilayers initially presenting 120 (*A*, *B*), 300 (*C*, *D*) and 1,000 (*E*, *F*) LFA-3 mol/μm^2. The pre-bleach line scans vividly display the relationship between initial LFA-3 density in the bilayer and peak LFA-3 accumulation in contact areas. FITC–LFA-3 in planar bilayers reconsti-

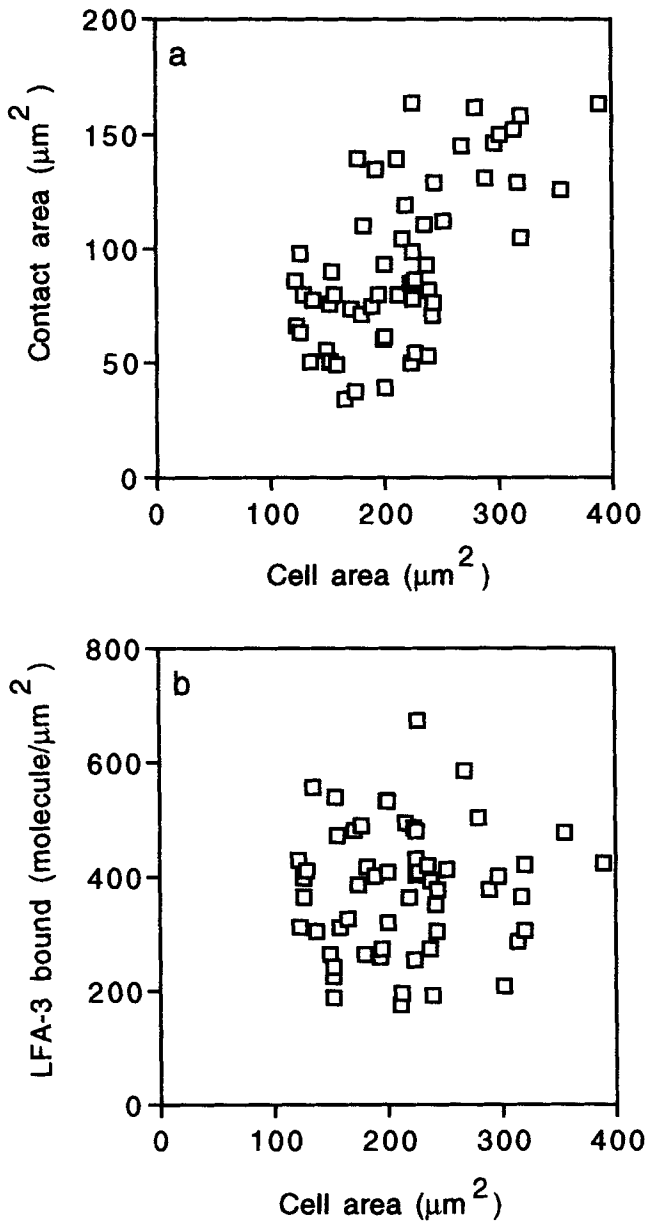

Figure 3. Cell size dependence of FITC–LFA-3 redistribution in planar bilayers initially presenting 1,000 LFA-3 mol/μm². Jurkat cells were allowed to adhere to planar egg PC bilayers containing FITC–LFA-3. Fluorescence images were analyzed for (*a*) size of contact area (μm²) and (*b*) density of bound FITC–LFA-3 in contact area (mol/μm²) as a function of projected cell area obtained from matched bright field images. Each symbol represents data from a single adherent cell.

tuted at 1,000 mol/μm² had a lateral diffusion coefficient of 5.9×10^{-9} cm²/s and a fractional mobility of 72% (Table I), in agreement with our previous observations (9). The diffusion coefficient of FITC-LFA-3 was decreased by 50–75% in areas of contact with Jurkat cells (Table I). The fractional mobility remained high in contact areas, as indicated by the nearly complete recovery of FITC–LFA-3 fluorescence after photobleaching of a contact area (Figs. 4 and 5, Table I).

Determination of Equilibrium Binding Parameters: Two-Dimensional Scatchard Analysis

The density and total number of bound and free FITC–LFA-3 molecules in contact areas between Jurkat cells and planar bilayers were analyzed by methods that are routinely applied to solution-phase equilibrium dialysis data. In the latter technique, receptors are restricted to a subregion by a semipermeable membrane, and small ligands capable of diffusion through the membrane undergo net concentration on the side of the membrane that contains a specific receptor (43). The adhesion experiment here was modeled as a two-dimensional version of the equilibrium dialysis experiment, in which CD2 and LFA-3 molecules were spatially restricted by the Jurkat cell plasma membrane and the planar bilayer, respectively. Table II summarizes the equilibrium surface density and total number of free FITC–LFA-3 molecules in non-contact regions, and of bound FITC–LFA-3 molecules in regions of cell-bilayer contact, for three initial FITC-LFA-3 densities. It should be noted that the three experimental FITC-LFA-3 surface densities span the physiological range in biological membranes. Data from Table II were transformed into a plot of bound LFA-3/free LFA-3 on the ordinate and bound LFA-3 on the abscissa (35) (Fig. 6). The three points fell on a line with a negative reciprocal slope (K_d) of 21 mol/μm² and an intercept on the abscissa (B_{max}) of 430 mol/μm². This analysis predicts that, since the density of CD2 on a T cell is on the order of 100 mol/μm², the CD2/LFA-3 interaction in biological membranes will be driven toward saturation upon establishment of cell–cell contact.

Discussion

We have used glass-supported planar phospholipid bilayers reconstituted with defined surface densities of laterally mobile FITC–LFA-3 to quantify the interaction between CD2 and LFA-3 in a model cell–cell contact area. Analysis of LFA-3 surface distribution and lateral mobility in the presence of $CD2^+$ Jurkat T cells reveals time-dependent redistribution of LFA-3 into contact sites and slowing of LFA-3 diffusion. Redistribution of LFA-3 reaches steady-state in 30 min and is maintained for several hours. At low densities of GPI–LFA-3 in planar bilayers adhesion of Jurkat cells increases dramatically between 5 and 20 min of incubation (9), consistent with the time-course of LFA-3 accumulation observed here. At higher GPI–LFA-3 densities adhesion of Jurkat cells is stable at 5 min (9), although redistribution of LFA-3 into contact areas does not reach steady-state until 30 min of incubation, suggesting that formation of a sufficient number of CD2/LFA-3 complexes to stabilize the contacts occurs before the system reaches equilibrium. These results are in qualitative agreement with those of McCloskey and Poo (26), who found that adhesion molecule (antibody–DNP complex) redistribution is closely associated with adhesion strengthening. We extend the results of McCloskey and Poo (26) on a high-affinity antibody/hapten interaction (solution-phase K_d = 10^{-8} M) to an interaction between adhesion molecules with a much higher solution-phase K_d (1.6×10^{-5} M) (44).

Our results indicate that CD2 in Jurkat cell membranes, like LFA-3 in the planar bilayers, also accumulates in con-

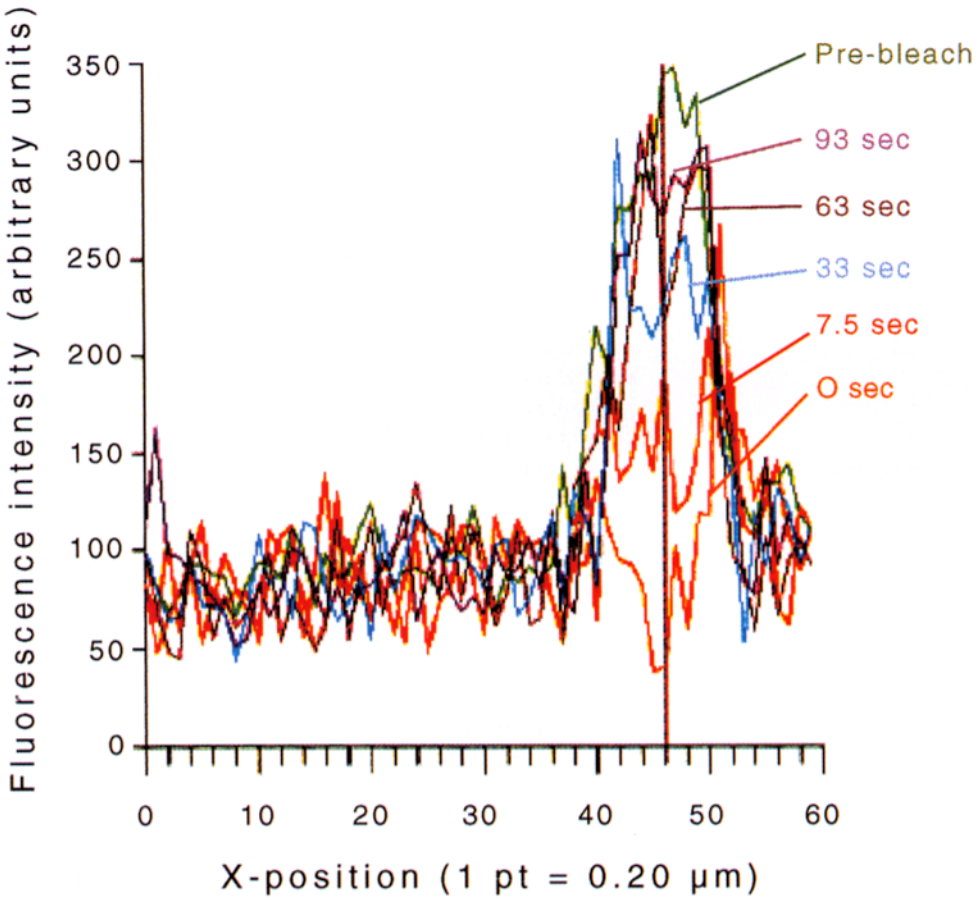

Figure 4. Accumulation and lateral mobility of FITC–LFA-3 in a region of contact with a Jurkat T cell. Jurkat cells were allowed to settle on a bilayer initially presenting 120 LFA-3 mol/μm^2 for 30 min at 24°C. The ACAS 570 was used to monitor fluorescence on a line passing through the center of a cell. The prebleach scan (*green*) shows FITC–LFA-3 accumulation in the contact area. The vertical line indicates the center of the bleaching spot, which was used to initiate a fluorescence photobleaching recovery experiment. Fluorescence recovery was monitored by line scans at 0 (*orange*), 1.5, 3, 4.5, 6, 7.5 (*red*), 9, 15, 21, 27, 33 (*blue*), 39, 45, 51, 57, 63 (*dark red*), 69, 75, 81, 87, and 93 (*purple*) seconds after the bleach. Diffusion coefficient, 1.0×10^{-9} cm^2/s. Fractional mobility, 85%.

tact areas. There are ~160,000 CD2 molecules on an average Jurkat T cell (33), and ~43,000 are engaged in an average contact area at steady-state. CD2 molecules are uniformly distributed on Jurkat cells in suspension (unpublished observations), yielding an initial CD2 surface density between 100 and 200 mol/μm^2. The maximum density of bound FITC–LFA-3 within a contact area, which should correspond exactly to the density of bound CD2 within the contact site, is 1,000 mol/μm^2. Thus, CD2 redistributes by a maximum of 5–10-fold in contact areas. Consistent with this observation, T cell CD2 is found to redistribute into areas of contact with cells expressing high levels of LFA-3 (30).

FITC–LFA-3 in a contact area manifests a reduced lateral diffusion coefficient compared to FITC–LFA-3 outside a contact area. Equilibrium binding of 83% of LFA-3 molecules to CD2 within a contact area causes the diffusion coefficient of LFA-3 to decrease from 5.9×10^{-9} cm^2/s to 1.3×10^{-9} cm^2/s. One explanation for this finding could be that CD2/LFA-3 complexes have a diffusion coefficient similar to that of CD2 in the Jurkat cell membrane (7.2×10^{-10} cm^2/s) (23). The suggestion that adhesion receptor/counter-receptor complexes diffuse laterally is intriguing, but may be difficult to establish in this system due to the rapid off-rate (>4 s^{-1}) of the CD2/LFA-3 interaction measured in solution (45). Nearly complete fluorescence recovery is observed even when most of the accumulated FITC–LFA-3 in a contact area is bleached, suggesting that bleached FITC–LFA-3 is replaced by fresh FITC–LFA-3 from the bilayer outside the contact area. This result suggests that transient interactions (19) between CD2 and LFA-3, even in the confines of the contact area, are a more likely explanation for the observed lateral diffusion of LFA-3 than the coupled diffusion of long-lived CD2/LFA-3 complexes.

The binding interaction responsible for the accumulation of LFA-3 in contact areas was analyzed by methods used to analyze interactions between soluble ligands and receptors (35). We obtained a two-dimensional K_d of 21 mol/μm^2, although the lowest initial LFA-3 density in bilayers was 120 mol/μm^2. It was not possible to perform equilibrium experiments using planar bilayers initially presenting fewer than 120 mol/μm^2, because such experiments resulted in surface densities of free FITC–LFA-3 in non-contact regions that were below the fluorescence detection limits of the ACAS 570. Thus, it is not possible to conclude from the Scatchard analysis whether the CD2/LFA-3 interaction exhibits one or more than one class of binding sites. The region of the Scatchard plot sampled here spans the range of physiological LFA-3 surface densities, however, and should be relevant to CD2/LFA-3 interactions in biological membranes. Furthermore, the region of the Scatchard plot near the abscissa typically describes the lowest affinity (highest capacity) sites. Thus, if more than one class of sites is present, the experiments reported here should yield an upper limit for the two-dimensional K_d of the CD2/LFA-3 interaction. Because physiological surface densities of LFA-3 exceed our experimentally de-

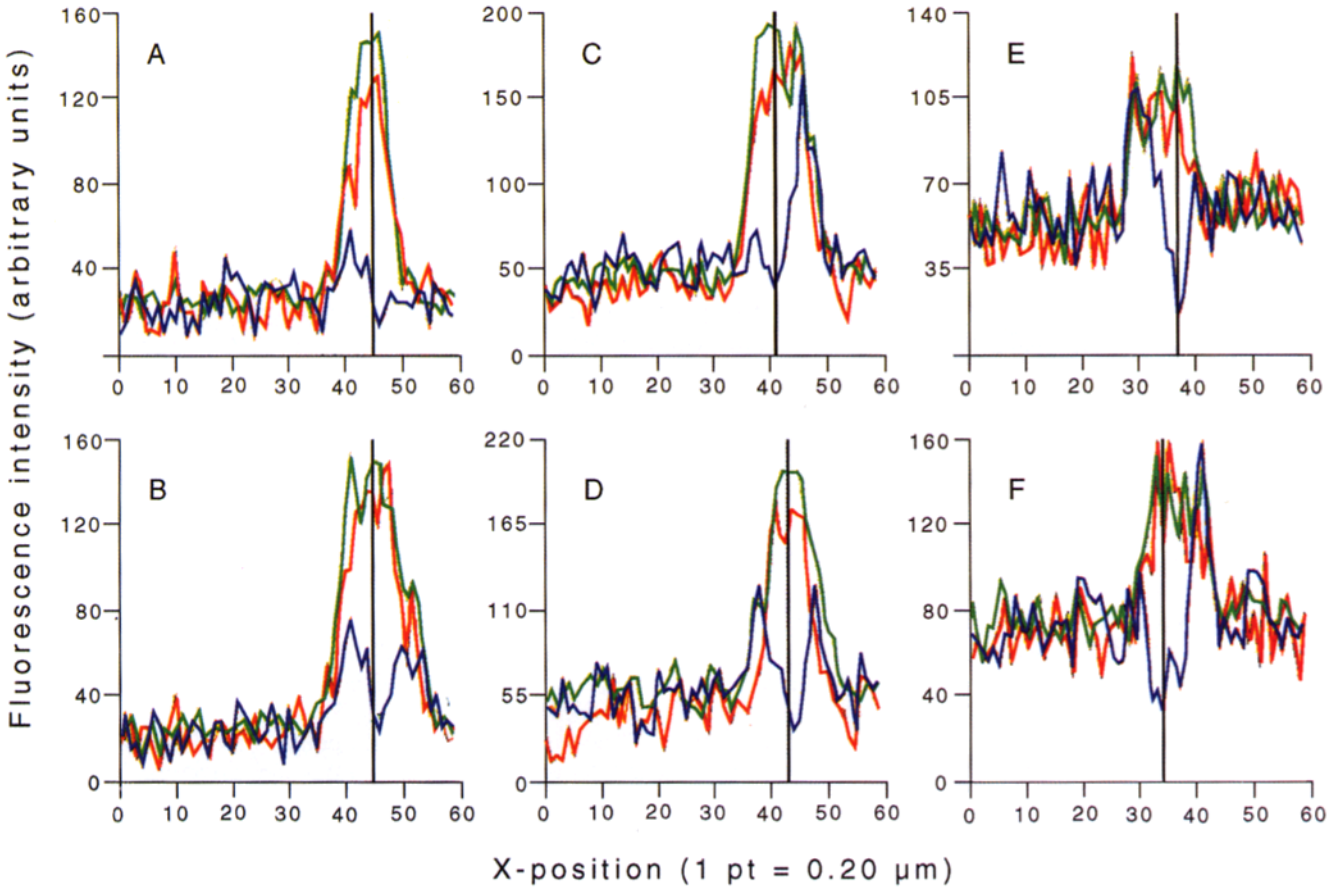

Figure 5. Accumulation and lateral mobility of FITC–LFA-3 in regions of contact between Jurkat cells and planar bilayers containing different initial densities of FITC–LFA-3. Jurkat cells were allowed to settle on bilayers initially presenting 120 (*A* and *B*), 300 (*C* and *D*), or 1,000 (*E* and *F*) LFA-3 mol/μm^2 for 30–120 min at 24°C. Prebleach (*green*), 0 s post-bleach (*blue*) and 90 s post-bleach (*red*) scans are shown to indicate the extents of FITC–LFA-3 accumulation, FITC–LFA-3 bleaching and FITC–LFA-3 fluorescence recovery, respectively. To minimize photobleaching during the fluorescence recovery phase of the experiment, the laser power and photomultiplier tube gain were adjusted for each bilayer to yield an acceptable signal level using minimal monitor beam power. Therefore, fluorescence intensity levels are not directly comparable among the various bilayer samples.

termined lower limit for the half-saturation point (K_d) of CD2/LFA-3 binding, the physiological CD2/LFA-3 system appears to operate near saturation once a contact area is formed.

The two-dimensional K_d measured here should take into account all active and passive contributions of the Jurkat cells to the CD2 affinity for LFA-3. Adhesion is thought to be regulated by a number of cellular processes, such as the association of adhesion receptors with the cytoskeleton and receptor clustering. It is not clear whether these active contributions modulate the two-dimensional K_d, however. To compare the measured two- and three-dimensional K_ds for the CD2/LFA-3 interaction, we make the conservative assumptions that the Ig-like domains of CD2 are conformationally fixed and that the soluble recombinant molecules used by van der Merwe and colleagues to assess the three-dimensional K_d (45) are identical in unitary interaction to the cell surface CD2 and

Table I. Lateral Mobility of FITC–LFA-3 in Regions of Contact between Planar Bilayers and Jurkat T Cells

Sample	Density*	*f*	*D*	B/Tot.‡	*n*
FITC–LFA-3 in egg PC, no cells present	1,000 and 300§	72 ± 15‖	5.9 ± 2.9	—	38
FITC–LFA-3 in egg PC, Jurkat cells present	1,000	88 ± 10	2.8 ± 1.6	31%	42
"	300	84 ± 14	2.3 ± 1.5	63%	31
"	120	83 ± 13	1.3 ± 0.9	83%	63

f, Fractional mobility, %. *D*, Diffusion coefficient, $\times 10^9$ cm^2/s. *n*, Number of measurements.
* Initial surface density, FITC–LFA-3 mol/μm^2.
‡ Bound LFA-3 molecules/total LFA-3 molecules in contact site.
§ Mobility data in the absence of cells were identical for bilayers containing LFA-3 at medium (300 μm^{-2}) and high (1,000 μm^{-2}) surface densities.
‖ Mean ± SD.

Table II. Redistribution of FITC–LFA–3 into Regions of Contact between Planar Bilayers and Jurkat T Cells

Initial LFA–3 surface density*	Equilibrium surface density of LFA–3 in non-contact regions	N	Equilibrium surface density of bound LFA–3 in contact regions‡	(B + F) /F§	Equilibrium number of bound LFA–3 molecules per cell × 10^{-4}‖	*n*
1,000	950 ± 149¶	4	430 ± 94	1.4	4.3 ± 2.0	28
300	250 ± 31	4	390 ± 183	2.6	3.9 ± 2.5	26
120	68 ± 15	5	330 ± 135	5.9	3.2 ± 1.7	49

Data include all measurements performed on membranes incubated with cells for at least 1 h (bilayers initially containing LFA–3 at 120 mol/μm² and 1,000 mol/μm²) or at least 30 min (bilayers initially containing 300 LFA–3 mol/μm²). *N*, number of planar bilayers. *n*, Number of cells.

* FITC–LFA–3 mol/μm².

‡ Bound LFA–3 mol/μm² in correct areas.

§ Accumulation of LFA–3 in contact areas defined as the total (bound plus free) density of LFA–3 in a contact area divided by the density of LFA–3 in areas of membrane not in contact with cells.

‖ Bound LFA–3 molecules per cell, $\times 10^{-4}$.

¶ Mean ± SD.

purified LFA-3 used in this study. We also assume that clustering of CD2 on the T cell does not alter the two-dimensional K_d, although such clustering may alter adhesion properties (47). Our analysis therefore considers, as a first approximation, only geometric properties of the contact area.

Bell and colleagues have suggested on theoretical grounds that the binding sites of adhesion molecules in a contact area may be limited to a "confinement region" (3, 4). While this is an intriguing possibility, the concept has not been experimentally tested. The height of the confinement region (σ) can be calculated from the following relationship (4):

$$\sigma\ (\mu m) = (K_{d_{x,y}}\ (mol/\mu m^2) \times 10^{15}\ \mu m^3/dm^3) \div (K_{d_{x,y,z}}\ (mol/dm^3) \times N_A\ (mol/mol))$$

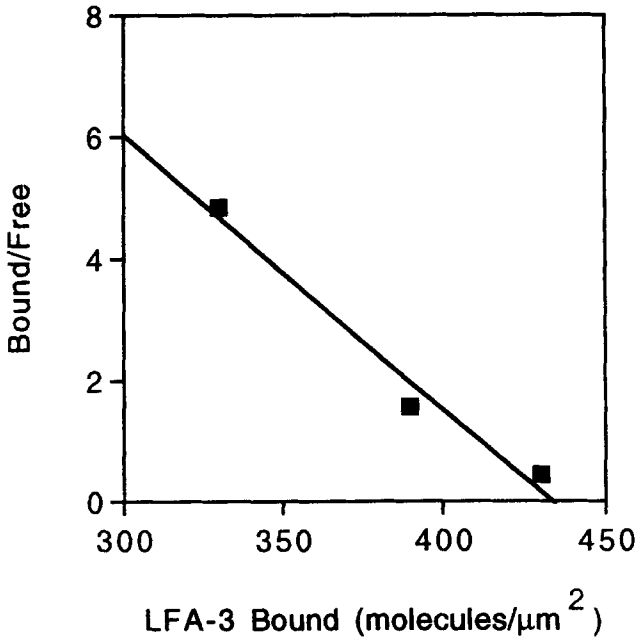

Figure 6. Scatchard analysis of binding between CD2 in Jurkat cell membranes and FITC-LFA-3 in planar bilayers. Data from Table II were transformed to bound LFA-3 and bound LFA-3/free LFA-3 and plotted as described in Materials and Methods. K_d = 21 ± 4 mol/μm². B_{max} = 430 ± 10 mol/μm². Errors were determined by using a linear regression program (Regression, version M1.23; Blackwell Scientific Publications, Oxford, UK).

where $K_{d_{x,y}}$ is the two-dimensional K_d, $K_{d_{x,y,z}}$ is the three-dimensional K_d, N_A is Avogadro's number and 1 l = 1 dm³. Using the two-dimensional K_d of 21 mol/μm² and the three-dimensional K_d of 6 μM (13) (where both K_ds are measured at room temperature), the calculated size of the confinement region for the CD2/LFA-3 interaction is 5.8 nm. Our data provide strong support for the confinement region concept. If LFA-3 molecules were separated in the direction normal to the membrane by the same average distance as in the plane of the membrane, then the average separation distance would be 220 nm rather than 5.8 nm. Thus, confinement generates an effective increase in three-dimensional affinity of 220 nm/5.8 nm, or 38-fold. Conversely, the average spacing of molecules at the three-dimensional K_d of 6 μM predicts a two-dimensional K_d of 230 mol/μm². The effective increase in two-dimensional affinity due to confinement is therefore 230 mol/μm²/21 mol/μm², or 11-fold. Note that the 38-fold increase in three-dimensional affinity is related to the 11-fold increase in two-dimensional affinity by the geometric relationship $38^{2/3} = 11$. The decrease in two-dimensional K_d, generated by limitation of the CD2/LFA-3 interaction to a confinement region, appears to be important in maximizing binding between CD2 and LFA-3 at physiologic densities on cell surfaces. Since cells with a high surface density of CD2 and LFA-3 express on the order of 100 mol/μm² (9, 25, 33, 37), and surface densities of LFA-3 can range considerably lower than this value (38), loss of the effect of confinement would result, at equilibrium, in a significant reduction in bond formation and a consequent reduction in adhesion strength.

Our observations may also provide a physical basis for the finding that CD2 and LFA-3 are often coexpressed on the same cell, yet do not appear to interact in *cis*, i.e., in the plane of the same membrane (17,37). The crystal structure of CD2 suggests that bilayers interacting through CD2/LFA-3 bonds are separated by ~15 nm (20,46). The smaller size of the confinement region for the CD2/LFA-3 interaction (i.e., 5.8 nm) could suggest that CD2 and LFA-3 are topologically constrained so that the angle formed between the long axis of either molecule and a line perpendicular to the bilayer is limited to values that allow the binding surfaces to remain in the confinement region. If each molecule is constrained to a confinement region of σ (5.8 nm), the long axis of each molecule has length L (7.5 nm for CD2), and the two molecules interact head-to-head through their NH_2-terminal Ig-like domains, then the an-

gle of confinement (Θ) can be calculated using the relationship:

$$\Theta = \cos^{-1}[(L - (\sigma \div 2)) \div L].$$

For CD2 and LFA-3 the calculated angle of confinement is ~52°. The mechanism by which the motion of CD2 or LFA-3 would be confined to the cone defined by this angle is unknown; it could, for example, involve interaction of the membrane proximal domain with the bilayer or of the entire molecule with the glycocalyx and neighboring glycoproteins. Of note, the stalk region of six amino acid residues that joins the COOH-terminus of IgSF domain 2 to the transmembrane segment is highly conserved among CD2 molecules in different species, suggesting that this region has an important function (42). The crystal structure of CD2 suggests that a confinement angle >65° would be required for *cis* interactions to occur (20). Thus, our findings may provide a physical explanation consistent with the observation that *cis*, non-adhesion promoting, interactions do not compete with *trans*, adhesion promoting, interactions. Further, CD2 and LFA-3 are homologous (36), are closely linked genetically (50), interact through homologous binding surfaces (46), and are postulated to have evolved from a common ancestor that interacted as a homodimer through *cis* interactions (49). Prevention of *cis* interactions of the common ancestor by topological constraints, as manifested in the confinement angle, could have been critical in permitting the evolution of adhesive *trans* interactions, in analogy to the CD2:CD2 interaction seen in the CD2 crystal structure (20). We note that the calculated confinement distance of 5.8 nm and the predicted membrane separation of 15 nm differ by only 2.6-fold. If either the two-dimension K_d measured here or the three-dimensional K_d measured by Davis et al. (13) is in error by this amount, then the argument for a confinement angle would disappear.

The notion of a confinement region for adhesion receptors has implications for adhesive interactions mediated by receptors of similar or dissimilar size. The CD2/LFA-3 interaction occurs naturally along side other adhesion receptor interactions, including those involving LFA-1/ICAM-1 and antigen receptors such as the T cell receptor (TCR) and CD16 (a low-affinity IgG Fc receptor). It has been pointed out (40, 46) that the molecular dimensions of CD2 and LFA-3 (20, 46) are similar to those predicted for the TCR (12) and MHC proteins (6, 8), suggesting that CD2 and LFA-3 may be effective in establishing a contact environment in which the TCR can function optimally. In contrast, LFA-1 and ICAM-1 appear capable of mediating adhesion with a larger intercellular distance than that preferred by the CD2/LFA-3 or TCR/MHC protein interaction. Contact areas involving LFA-1 and ICAM-1 could be physically segregated (i.e., laterally separated) from areas containing CD2/LFA-3 and TCR/MHC proteins, allowing each system to maintain an optimal cell–cell separation distance and confinement region. Adhesion receptors with strikingly different geometries have been described: adhesion may be regulated in some systems by changes in intercellular distance (44).

We have described a novel approach to the molecular analysis of adhesion molecule interactions in a contact area. The results allow calculation of a two-dimensional K_d that relates directly to the natural function of these molecules in adhesion. Our findings demonstrate that a three-dimensional K_d must be interpreted in the context of additional topological constraints on adhesion molecules in a membrane environment to determine the relationship between two-dimensional and three-dimensional K_ds. In fact, both the two- and three-dimensional K_ds must be known to characterize fully the interaction of adhesion molecules.

M. L. Dustin thanks Drs. E. Unanue and S. Tietelbaum for their support. We thank Dr. J. Caulfield for helpful discussions.

This work was supported by National Institutes of Health grants CA31798 (T. A. Springer), HL15157, and HL32854 (D. E. Golan).

Recieved for publication 28 August and in revised form 3 November 1995.

References

1. Arulanandam, A. R. N., J. M. Withka, D. F. Wyss, G. Wagner, A. Kister, P. Pallai, M. A. Recny, and E. L. Reinherz. 1993. The CD58 (LFA-3) binding site is a localized and highly charged surface area on the AGFCC'C" face of the human CD2 adhesion domain. *Proc. Natl. Acad. Sci. USA.* 90: 11613–11617.
2. Axelrod, D., D. E. Koppel, J. Schlessinger, E. L. Elson, and W. W. Webb. 1976. Mobility measurement by analysis of fluorescence photobleaching recovery kinetics. *Biophys. J.* 16:1055–1069.
3. Bell, G. I. 1978. Models for the specific adhesion of cells to cells. A theoretical framework for adhesion mediated by reversible bonds between cell surface molecules. *Science (Wash. DC).* 200:618–627.
4. Bell, G. I., M. Dembo, and P. Bongrand. 1984. Cell adhesion: competition between nonspecific repulsion and specific binding. *Biophys. J.* 45:1051–1064.
5. Bevington, P. R. 1969. Data reduction and error analysis for the physical sciences. McGraw-Hill, Inc., NY. 336 pp.
6. Bjorkman, P. J., M. A. Saper, B. Samraoui, W. S. Bennett, J. L. Strominger, and D. C. Wiley. 1987. Structure of the human class I histocompatibility antigen, HLA-A2. *Nature (Lond.).* 329:506–512.
7. Brian, A. A., and H. M. McConnell. 1984. Allogeneic stimulation of cytotoxic T cells by supported planar membranes. *Proc. Natl. Acad. Sci. USA.* 81:6159–6163.
8. Brown, J. H., T. S. Jardetzky, J. C. Gorga, L. J. Stern, R. G. Urban, J. L. Strominger, and D. C. Wiley. 1993. Three-dimensional structure of the human class II histocompatibility antigen HLA-DR1. *Nature (Lond.).* 364:33–39.
9. Chan, P.-Y., M. B. Lawrence, M. L. Dustin, L. M. Ferguson, D. E. Golan, and T. A. Springer. 1991. The influence of receptor lateral mobility on adhesion strengthening between membranes containing LFA-3 and CD2. *J. Cell Biol.* 115:245–255.
10. Chen, W. T., T. Hasegawa, C. Hasegawa, C. Weinstock, and K. M. Yamada. 1985. Development of cell surface linkage complexes in cultivated fibroblasts. *J. Cell Biol.* 100:1103–1114.
11. Damsky, C. H., K. A. Knudsen, D. Bradley, C. A. Buck, and A. F. Horwitz. 1985. Distribution of the cell substratum attachment (CSAT) antigen on myogenic and fibroblastic cells in culture. *J. Cell Biol.* 100:1528–1539.
12. Davis, M. M., and P. J. Bjorkman. 1988. T-cell antigen receptor genes and T-cell recognition. *Nature (Lond.).* 334:395–402.
13. Davis, S. J., E. A. Davies, A. N. Barclay, S. Daenke, D. L. Bodian, E. Y. Jones, D. I. Stuart, T. D. Butters, R. A. Dwek, and P. A. van der Merwe. 1995. Ligand binding by the immunoglobulin superfamily recognition molecule CD2 is glycosylation-independent. *J. Biol. Chem.* 270:369–375.
14. de Fougerolles, A. R., and T. A. Springer. 1991. ICAM-3, a third adhesion counter-receptor for LFA-1 on resting lymphocytes. *J. Exp. Med.* 175: 185–195.
15. Doyle, C., and J. L. Strominger. 1987. Interaction between CD4 and class II MHC molecules mediates cell adhesion. *Nature (Lond.).* 330:256–259.
16. Dustin, M. L., O. Carpén, and T. A. Springer. 1992. Regulation of locomotion and cell-cell contact area by the LFA-1 and ICAM-1 adhesion receptors. *J. Immunol.* 148:2654–2663.
17. Dustin, M. L., M. E. Sanders, S. Shaw, and T. A. Springer. 1987. Purified lymphocyte function-associated antigen-3 (LFA-3) binds to CD2 and mediates T lymphocyte adhesion. *J. Exp. Med.* 165:677–692.
18. Dustin, M. L., and T. A. Springer. 1991. Role of lymphocyte adhesion receptors in transient interactions and cell locomotion. *Annu. Rev. Immunol.* 9:27–66.
19. Elson, E. L., and H. Qian. 1989. Interpretation of fluorescence correlation spectroscopy and photobleaching recovery in terms of molecular interactions. *Methods Cell Biol.* 30:307–332.
20. Jones, E. Y., S. J. Davis, A. F. Williams, K. Harlos, and D. I. Stuart. 1992.

Crystal structure at 2.8 A resolution of a soluble form of the cell adhesion molecule CD2. *Nature (Lond.)*. 360:232–239.
21. Kinch, M. S., A. Sanfridson, and C. Doyle. 1994. The protein tyrosine kinase p56lck regulates cell adhesion mediated by CD4 and major histocompatibility complex class II proteins. *J. Exp. Med.* 180:1729–1739.
22. Kupfer, A., and S. J. Singer. 1989. The specific interaction of helper T cells and antigen-presenting B cells. IV. Membrane and cytoskeletal reorganizations in the bound T cell as a function of antigen dose. *J. Exp. Med.* 170:1697–1713.
23. Liu, S. J., W. C. Hahn, B. E. Bierer, and D. E. Golan. 1995. Intracellular mediators regulate CD2 lateral diffusion and cytoplasmic calcium ion mobilization upon CD2-mediated T cell activation. *Biophys. J.* 68:459–470.
24. Luescher, I. F., E. Vivier, A. Layer, J. Mahiou, F. Godeau, B. Malissen, and P. Romero. 1995. CD8 modulation of T-cell antigen receptor-ligand interactions on living cytotoxic T lymphocytes. *Nature (Lond.)*. 373:353–356.
25. Martin, P. J., G. Longton, J. A. Ledbetter, W. Newman, M. P. Braun, P. G. Beatty, and J. A. Hansen. 1983. Identification and functional characterization of two distinct epitopes on the human T cell surface protein Tp50. *J. Immunol.* 131:180–185.
26. McCloskey, M. A., and M. M. Poo. 1986. Contact-induced redistribution of specific membrane components: local accumulation and development of adhesion. *J. Cell Biol.* 102:2185–2196.
27. McConnell, H. M., T. H. Watts, R. M. Weis, and A. A. Brian. 1986. Supported planar membranes in studies of cell-cell recognition in the immune system. *Biochim. Biophys. Acta.* 864:95–106.
28. Michl, J., M. M. Pieczonka, J. C. Unkeless, G. I. Bell, and S. C. Silverstein. 1983. Fc receptor modulation in mononuclear phagocytes maintained on immobilized immune complexes occurs by diffusion of the receptor molecule. *J. Exp. Med.* 157:2121–2139.
29. Mimms, L. T., G. Zampighi, Y. Nozaki, C. Tanford, and J. A. Reynolds. 1981. Phosholipid vesicle formation and transmembrane protein incorporation using octyl glucoside. *Biochemistry*. 20:833–840.
30. Moingeon, P. E., J. L. Lucich, C. C. Stebbins, M. A. Recny, B. P. Wallner, S. Koyasu, and E. L. Reinherz. 1991. Complementary roles for CD2 and LFA-1 adhesion pathways during T cell activation. *Eur. J. Immunol.* 21: 605–610.
31. O'Rourke, A. M., J. R. Apgar, K. P. Kane, E. Martz, and M. F. Mescher. 1991. Cytoskeletal function in CD8- and T cell receptor-mediated interaction of cytotoxic T lymphocytes with class I protein. *J. Exp. Med.* 173: 241–249.
32. Peterson, A., and B. Seed. 1987. Monoclonal antibody and ligand binding sites of the T cell erythrocyte receptor (CD2). *Nature (Lond.)*. 329:842–846.
33. Plunkett, M. L., and T. A. Springer. 1986. Purification and characterization of the lymphocyte function-associated-2 (LFA-2) molecule. *J. Immunol.* 136:4181–4187.
34. Sanchez-Madrid, F., A. M. Krensky, C. F. Ware, E. Robbins, J. L. Strominger, S. J. Burakoff, and T. A. Springer. 1982. Three distinct antigens associated with human T lymphocyte-mediated cytolysis: LFA-1, LFA-2, and LFA-3. *Proc. Natl. Acad. Sci. USA*. 79:7489–7493.
35. Scatchard, G. 1949. The attractions of proteins for small molecules and ions. *Ann. NY Acad. Sci.* 51:660–672.
36. Seed, B. 1987. An LFA-3 cDNA encodes a phospholipid-linked membrane protein homologous to its receptor CD2. *Nature (Lond.)*. 329:840–842.
37. Selvaraj, P., M. L. Plunkett, M. Dustin, M. E. Sanders, S. Shaw, and T. A. Springer. 1987. The T lymphocyte glycoprotein CD2 (LFA-2/T11/E-Rosette receptor) binds the cell surface ligand LFA-3. *Nature (Lond.)*. 326:400–403.
38. Shaw, S., G. G. Luce, W. R. Gilks, K. Anderson, K. Ault, B. S. Bochner, L. Boumsell, S. M. Denning, E. G. Engleman, T. Fleisher et al. 1995. Leucocyte differentiation antigen database. *In* Leucocyte Typing V: White Cell Differentiation Antigens. S. F. Schlossman, L. Boumsell, W. Gilks, J. M. Harlan, T. Kishimoto, C. Morimoto, J. Ritz, S. Shaw, R. Silverstein, T. Springer et al., editors. Oxford University Press, Oxford. 16–198.
39. Somoza, C., P. C. Driscoll, J. G. Cyster, and A. F. Williams. 1993. Mutational analysis of the CD2/CD58 interaction: the binding site for CD58 lies on one face of the first domain of human CD2. *J. Exp. Med.* 178:549–558.
40. Springer, T. A. 1990. Adhesion receptors of the immune system. *Nature (Lond.)*. 346:425–433.
41. Takai, Y., M. L. Reed, S. J. Burakoff, and S. H. Herrmann. 1987. Direct evidence for a receptor-ligand interaction between the T-cell surface antigen CD2 and lymphocyte-function-associated antigen 3. *Proc. Natl. Acad. Sci. USA*. 84:6864–6868.
42. Tavernor, A. S., J. H. Kydd, D. L. Bodian, E. Y. Jones, D. I. Stuart, S. J. Davis, and G. W. Butcher. 1994. Expression cloning of an equine T-lymphocyte glycoprotein CD2 cDNA. Structure-based analysis of conserved sequence elements. *Eur. J. Biochem.* 219:969–976.
43. Tong, P. Y., W. Gregory, and S. Kornfeld. 1989. Ligand interactions of the cation-independent mannose 6-phosphate receptor. The stoichiometry of mannose 6-phosphate binding. *J. Biol. Chem.* 264:7962–7969.
44. van der Merwe, P. A., and A. N. Barclay. 1994. Transient intercellular adhesion: the importance of weak protein-protein interactions. *Trends Biochem. Sci.* 19:354–358.
45. van der Merwe, P. A., A. N. Barclay, D. W. Mason, E. A. Davies, B. P. Morgan, M. Tone, A. K. C. Krishnam, C. Ianelli, and S. J. Davis. 1994. Human cell-adhesion molecule CD2 binds CD58 (LFA-3) with a very low affinity and an extremely fast dissociation rate but does not bind CD48 or CD59. *Biochemistry*. 33:10149–10160.
46. van der Merwe, P. A., P. N. McNamee, E. A. Davies, A. N. Barclay, and S. J. Davis. 1995. Topology of the CD2-CD48 cell-adhesion molecule complex: implications for antigen recognition by T cells. *Curr. Biol.* 5:74–84.
47. Ward, M. D., M. Dembo, and D. A. Hammer. 1994. Kinetics of cell detachment: peeling of discrete receptor clusters. *Biophys. J.* 67:2522–2534.
48. Weis, R. M., K. Balakrishnan, B. A. Smith, and H. M. McConnell. 1982. Stimulation of fluorescence in a small contact region between rat basophil leukemia cells and planar lipid membrane targets by coherent evanescent radiation. *J. Biol. Chem.* 257:6440–6445.
49. Williams, A. F., and A. N. Barclay. 1988. The immunoglobulin superfamily: domains for cell surface recognition. *Annu. Rev. Immunol.* 6:381–405.
50. Wong, Y. W., A. F. Williams, S. F. Kingsmore, and M. F. Seldin. 1990. Structure, expression, and genetic linkage of the mouse BCM1 (OX45 or Blast-1) antigen: evidence for genetic duplication giving rise to the BCM1 region on mouse chromosome 1 and the CD2/LFA-3 region on mouse chromosome 3. *J. Exp. Med.* 171:2115–2130.